Supporting Information for "Vibrational properties of $CuInP_2S_6$ across the ferroelectric transition"

Sabine N. Neal,[1] Sobhit Singh,[2] Xiaochen Fang,[3] Choongjae Won,[4] Fei-ting Huang,[5] Sang-Wook Cheong,[2,3,4] Karin M. Rabe,[2] David Vanderbilt,[2] and Janice L. Musfeldt[1,6,*]

[1]*Department of Chemistry, University of Tennessee, Knoxville, Tennessee 37996, USA*

[2]*Department of Physics and Astronomy, Rutgers University, Piscataway, New Jersey 08854, USA*

[3]*Rutgers Center for Emergent Materials, Rutgers University, Piscataway, new Jersey 08854, USA*

[4]*Laboratory for Pohang Emergent Materials and Max Plank POSTECH Center for Complex Phase Materials, Pohang University of Science and Technology, Pohang 790-784, Korea*

[5]*Rutgers Center for Emergent Materials, Rutgers University, Piscataway, New Jersey 08854, USA*

[6]*Department of Physics and Astronomy, University of Tennessee, Knoxville, Tennessee 37996, USA*

(Dated: August 5, 2021)

Visual appearance of the crystals and domain pattern details

Figure S1 shows a side by side comparison of two types of $CuInP_2S_6$ crystals that result from the same growth conditions. These crystals display distinct thicknesses, colors, and sizes, making it possible to tell them apart by visual inspection. For example, the type-I crystal [Fig. S1 (a) right and (c)] has a much larger lateral dimension (3-10 mm) as well as a reduced thickness (10-30 µm). This crystal is also lighter in color and displays a pattern of wavy stripes with dark/bright contrast. The type-II crystal [Fig. S1 (a) left and (b)] has a homogeneous orange color, small lateral dimension (0.5-1.0 mm), and a thickness of 70-150 µm. The type-I crystal type is mixed-phase $CuInP_2S_6$, whereas the type-II crystal is pure $CuInP_2S_6$.

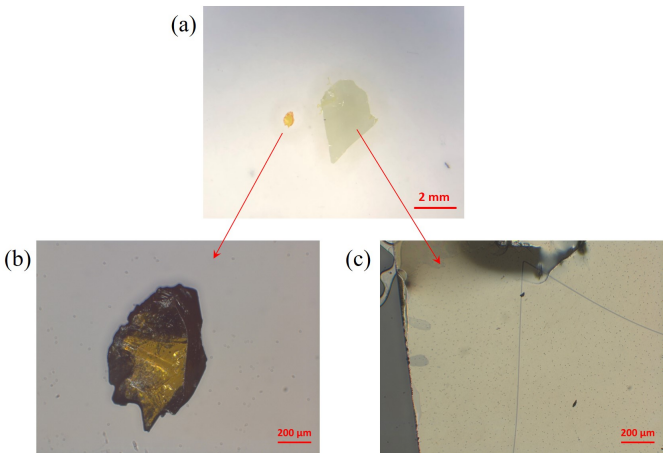

FIG. S1. (a) Size comparison of the different types of crystal flakes. (b,c) 5× Optical microscope images taken in bright field mode of (b) the type of flake with small lateral dimension and greater thickness (corresponding to the pure phase system) and (c) the type of flake with large lateral dimension and lesser thickness (corresponding to the mixed phase system).

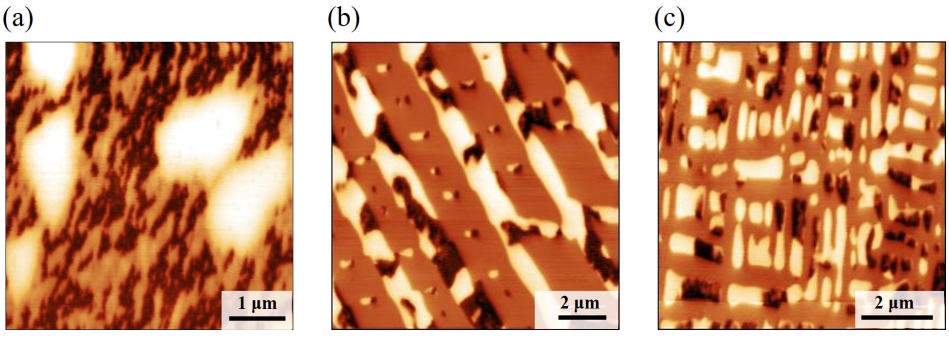

FIG. S2. Vertical piezo-force microscopy images of (a) phase-separated $CuInP_2S_6$ showing impurity phase with circular shape, (b) phase-separated $CuInP_2S_6$ showing straight stripe patterns, (c) phase-separated $CuInP_2S_6$ showing rectangular block patterns.

* musfeldt@utk.edu

Figure S2 displays the vertical piezoforce microscopy images revealing how pure $CuInP_2S_6$ and $In_{4/3}P_2S_6$ coexist to yield a mixed phase crystal. The phase-separated patterns vary a great deal and include alternating wavy stripes with circular impurity inclusions (a), straight stripes (b), and rectangular blocks (c). The phase separation appears to be quite robust with domain size depending upon cooling rates.

Vibrational mode assignments from lattice dynamics calculations

Tables S1 and S2 summarize our experimental and calculated infrared and Raman-active mode assignments for single crystalline $CuInP_2S_6$. A short description of each mode displacement pattern is included. Figure S3 summarizes a comparison between experimental and theoretical mode frequencies for the $C2/c$ and Cc space groups. Good agreement is observed between theoretical predictions and experimental observations.

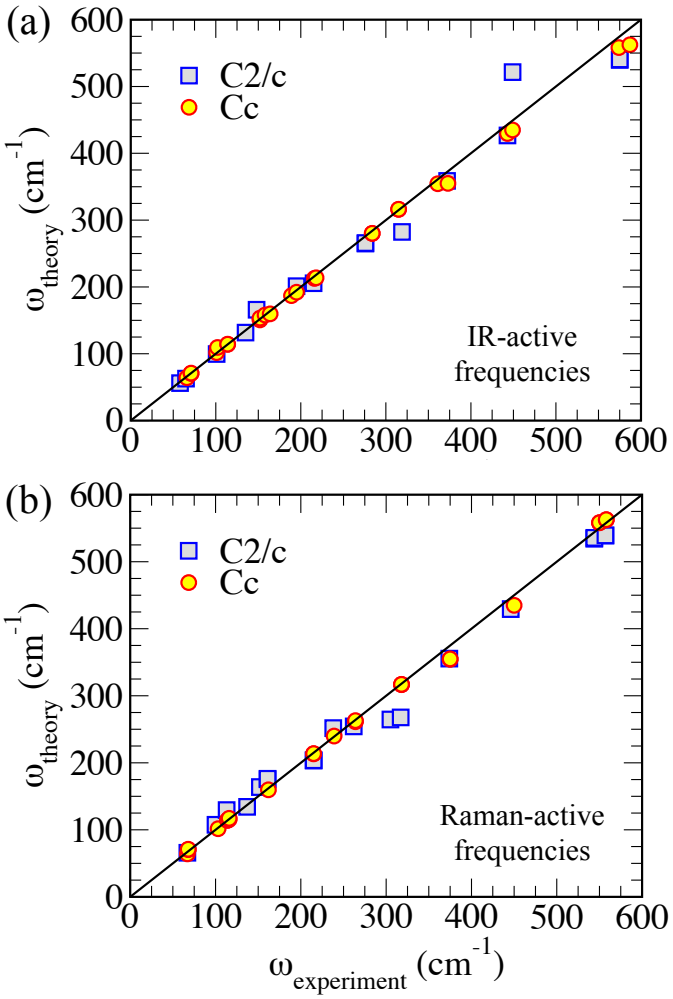

FIG. S3. Comparison of the experimental data recorded at 325 (≈ 300) K for $C2/c$ (Cc) phase of $CuInP_2S_6$ with the DFT-D3 calculated (a) infrared and (b) Raman-active phonon frequencies at 0 K. We note that LO-TO corrections were not considered in our DFT-D3 calculations, which are responsible for modest deviation of the theoretical data for infrared-active modes at higher frequencies from the diagonal line, *i.e.*, from the experimental data.

Hysteresis in the ferroelectric and structural transitions

Figure S4 displays variable temperature Raman measurements of $CuInP_2S_6$ with both increasing temperature (Panels a and c) and decreasing temperature (Panels b and d) across two frequency windows. The top panels highlight the features from 150 - 350 cm^{-1} and the bottom panels show the modes present over the 400 - 600 cm^{-1} range. Taking a closer look, there appears to be a two-step hysteresis associated with both the T_C and T_S transition regions. However, the ferroelectric transition changes only slightly, whereas the structural transition temperature shows a dramatic change related dependently to the direction of measurement. For example, when measurements were taken with increasing temperature, the T_S increases and the two-step transition region narrows. The opposite is also true. When

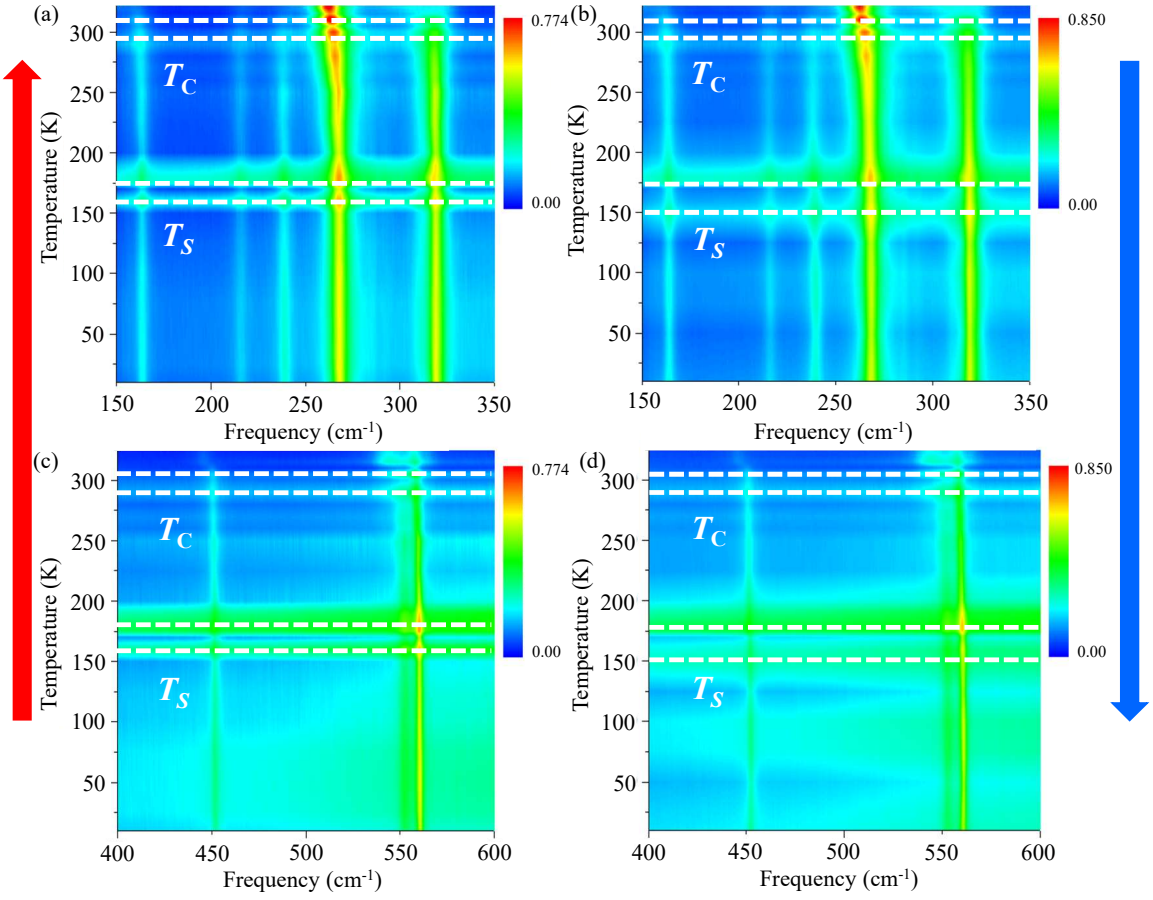

FIG. S4. Hysteresis effects in the Raman scattering response of $CuInP_2S_6$. Panels (a, c) Raman measurements with increasing temperature; (b, d) with decreasing temperature. The top panels show features in the 150 - 350 cm^{-1} range, whereas the bottom panels highlight features in the 400 - 600 cm^{-1} range. The ferroelectric and structural transitions are indicated by the dashed-lines.

measuring with decreasing temperature, the structural transition decreases slightly and the area shows a broadening.

TABLE S1. Frequency of the infrared-active modes along with their vibrational assignments for single crystalline $CuInP_2S_6$. Corresponding DFT-D3 calculated mode frequencies are given in parentheses. All values are in units of cm^{-1}.

$C2/c$		Cc		
Exp. (Theory)	**Symmetry**	**Exp. (Theory)**	**Symmetry**	**Displacement patterns**
58 (56.1)	A_u	-	-	in-plane Cu + out-of-plane S vibration
65 (62.8)	B_u	-	-	in-plane twist of P-P dimers + out-of-plane S vibration
-	-	66 (64.2)	A'	out-of-plane polar displacement of Cu
-	-	71 (70.5, 71.0)	A', A''	in-plane displacement of Cu + In + P + out-of-plane S
101 (99.6)	B_u	101, 102 (101.7, 109.4)	A', A''	rigid out-of-plane displacement of P-P dimers (in-phase in adjacent layers for A', and opposite phase for A'')
-	-	114 (114.1, 114.3)	A', A''	in-plane Cu + In, and out-of-plane S vibration
135 (131.7)	B_u	-	-	in-plane S vibration
148 (165.9)	B_u	-	-	rigid out-of-plane displacement of P-P dimers (in-phase in adjacent layers) + in-plane S vibration
-	-	151 (150.7, 153.4)	A', A''	in-plane Cu + In + P-P dimers, and out-of-plane S vibration
-	-	158, 164 (158.0, 159.7)	A'', A'	out-of-plane displacement of P-P dimers + in-plane S vibration
-	-	189 (187.0)	A''	in-plane displacement of Cu + P-P dimers + out-of-plane S vibration
195, 215 (201.1, 205.5)	A_u, B_u	195, 216, 218 (192.1, 212.7, 213.7)	A', A', A''	in-plane Cu + P + out-of-plane S vibration
276 (264.9, 265.7)	B_u, A_u	-	-	in-plane Cu + S vibration
-	-	284 (280.0, 280.3)	A', A''	in-plane Cu + P + S vibrations
319 (282.3)	B_u	-	-	out-of-plane P-P translation + out-of-plane S vibration
-	-	315 (316.1, 316.3)	A', A''	in-plane Cu + P + S vibrations
-	-	361 (354.4)	A'	in-plane Cu + S and out-of-plane P-P stretching (in-phase in adjacent layers)
372 (358.7)	A_u	373 (355.0)	A''	in-plane Cu + S and out-of-plane P-P stretching (opposite phase in adjacent layers)
443 (426.7)	B_u	443 (429.6)	A'	out-of-plane P-P translation + in-plane S vibration
449 (521.5)	A_u	449 (434.9)	A''	out-of-plane P-P + in-plane S vibration
574 (539.7, 540.6)	B_u, A_u	574, 587, 611 (558.2, 562.5, 562.7)	A'', A', A''	in-plane P-P + in-plane S vibration

TABLE S2. Frequency of the Raman-active modes along with their vibrational assignments for single crystalline $CuInP_2S_6$. Corresponding DFT-D3 calculated mode frequencies are given in parentheses. All values are in units of cm^{-1}.

$C2/c$		Cc		
Exp. (Theory)	**Symmetry**	**Exp. (Theory)**	**Symmetry**	**Displacement patterns**
67 (65.8)	B_g	-	-	in-plane P + out-of-plane S vibration
-	-	68, 67 (64.2, 70.5, 71.0)	A', A'', A''	out-of-plane Cu (polar for A' and antipolar for A'' displacements in the adjacent layers) + out-of-plane S vibration
100 (107.5)	B_g	-	-	rigid out-of-plane displacement of P-P dimers (opposite phase in adjacent layers) + In displacements opposite to that of P-P dimers
-	-	103 (101.7)	A'	rigid out-of-plane displacement of P-P dimers (in-phase phase in adjacent layers) + In displacements opposite to that of P-P dimers
113 (129.5)	A_g	114, 116 (114.1, 114.3, 115.5, 117.2)	A', A'', A', A''	in-plane displacement of Cu + In + S, out-of-plane S vibration
137 (134.3)	B_g	-	-	in-plane displacement of Cu + In + S
152 (163.8)	B_g	-	-	rigid out-of-plane displacement of P-P dimers (in-phase in adjacent layers for A', and opposite phase for A'')
161 (175.4, 176.2)	A_g, A_g	-	-	in-plane Cu + P and out-of-plane S vibration
-	-	162 (159.7)	A'	out-of-plane P-P + in-plane S vibration
215 (203.4, 203.8)	B_g, A_g	215 (213.4, 213.7)	A', A''	in-plane Cu + P, and out-of-plane S vibration
238, 262 (251.7, 254.3)	B_g, A_g	239 (239.9)	A'	in-plane Cu + P, and out-of-plane S vibration
-	-	264 (261.3, 262.9)	A', A''	in-plane S vibration
305 (264.6)	A_g	-	-	in-plane S vibration
317 (267.7)	B_g	318 (316.6, 316.8, 317.0)	A'', A', A''	in-plane P + S vibration
374 (355.4)	A_g	375 (354.4, 355.0)	A', A''	out-of-plane P + in-plane S vibration
446 (429.3)	B_g	450 (434.9)	A''	out-of-plane P + out-of-plane S vibration
544 (534.2, 535.6)	A_g, B_g	550 (558.1, 558.2)	A'', A'	in-plane P-P stretching + in-plane S vibration
557 (539.0, 539.3)	A_g, B_g	558 (562.5, 562.7)	A', A''	in-plane P-P + in-plane S vibration